Composites Science and Technology 285 (2026) 111813

Contents lists available at ScienceDirect

Composites Science and Technology

journal homepage: www.elsevier.com/locate/compscitech

Development and experimental validation of strain rate-dependent failure criteria for unidirectional non-crimp fabric composites

Nils Koltzenburg [a,b], Khizar Rouf [a], Thomas Böhlke [b], John Montesano [a,*]

[a] Composites Research Group, Department of Mechanical and Mechatronics Engineering, University of Waterloo, 200 University Avenue West, Waterloo ON, N2L 3G1, Canada

[b] Institute of Engineering Mechanics, Karlsruhe Institute for Technology (KIT), Kaiserstraße 12, 76131 Karlsruhe, Germany

A R T I C L E I N F O

Keywords:
Unidirectional non-crimp fabric composites
Invariant-based failure criteria
Analytical modeling
Strain rate-dependency

A B S T R A C T

In this study, two invariant-based failure criteria are proposed to predict failure of a unidirectional non-crimp fabric (UD-NCF) carbon fiber/epoxy composite. Three different failure modes, namely matrix failure, fiber tensile failure, and fiber compressive failure, are considered. The matrix failure functions are based on linear and quadratic transversely isotropic stress-invariants, while fiber failure is evaluated with a maximum stress criterion for tension and an adapted kinking criterion for compression. The main advantages of the invariant-based criteria are fewer required experiments for calibration and minimal computational effort in comparison with fracture plane-based criteria. Moreover, the chosen mathematical formulation ensures a non-negative Hessian and decoupled tensile and compressive behavior. Furthermore, the strain rate dependency of the investigated UD-NCF composite is incorporated using empirical relations defined in previous work by the authors. For validation purposes, off-axis tests are performed at quasi-static and high strain rates. Overall, the observed agreement with experimental data presented here as well as from literature is excellent, highlighting the feasibility of the proposed criteria for design of UD-NCF composite structures.

1. Introduction

Carbon footprint reduction is a key focus in the transportation sector, with the adoption of fiber reinforced plastic (FRP) composites emerging as a prominent strategy for mass reduction and improved fuel efficiency owing to their high specific strength and stiffness. The superior energy absorption capabilities of FRP composites in comparison to conventional metallic alloys allows for significant improvement in vehicle crashworthiness performance and occupant safety [1], which must be predicted during the design process of associated structures. Impacted automobile structures can experience strain rates in excess of 300 s^{-1} [2]; thus, associated prediction models must account for the strain rate dependent strength of FRP composite materials. Predicting the impact performance of composite structures requires use of failure criteria; however, since the unidirectional (UD) plies of laminated FRPs are transversely isotropic, well known isotropic failure or yield criteria, such as the von Mises or Tresca criteria, cannot be used to adequately model failure. Therefore, appropriate ply-level or intra-ply failure criteria for composites have been investigated during the past several decades [3–16], which allow for a reduction of the testing effort and thus time and cost savings in the development process if the used failure criteria provide accurate predictions. In order to predict failure of multidirectional laminates, a degradation analysis is performed, most often on a ply-by-ply basis [17]. While there are various approaches in the field of damage mechanics for FRPs in the literature [18–21], that can be micromechanically motivated [19] or based on a probabilistic approach [20], for a ply-by-ply analysis it is important to model the underlying ply failure accurately.

Different intra-ply failure criteria for UD composites have been developed, including maximum stress [22] or strain [11] criteria, so called "interactive" criteria [5,6,16], which do not distinguish between failure modes, and "physically based" failure criteria [8,9,13–15], which distinguish at least between matrix and fiber failure (FF) modes. The latter criteria are regarded as being more robust for various types of UD composites under combined stress states as they account for distinct failure modes and, in general, consider the underlying local failure mechanisms [23]. FF is typically distinguished by both tensile and compressive failure. Matrix failure, also called inter-fiber failure (IFF), occurs due to fracture in a plane parallel to the fiber direction [9,24], where the orientation is assumed to be dependent on the magnitude and direction of transverse and shear stress components.

* Corresponding author.
E-mail addresses: nils.koltzenburg@alumni.kit.edu (N. Koltzenburg), krouf@uwaterloo.ca (K. Rouf), thomas.boehlke@kit.edu (T. Böhlke), john.montesano@uwaterloo.ca (J. Montesano).

https://doi.org/10.1016/j.compscitech.2026.111813
Received 1 July 2025; Received in revised form 8 December 2025; Accepted 9 August 2026
Available online 31 August 2026

The physically based failure criteria are generally distinguished by the IFF mode criteria.

IFF mode criteria that are based on the fracture plane concept require the determination of the fracture plane orientation [9,13], which is not analytically possible for general 3D stress states. Thus, different numerical optimization approaches have been commonly used [24–29]; however the numerical effort is, in general, computationally inefficient. The worldwide failure exercises (WWFEs) aimed to compare and assess the predictive capabilities of existing failure criteria [30–32]. While no single failure criterion showed an overall superior predictive capability, many researchers recommended use of the fracture plane concept despite its limitation. Another outcome of the WWFEs was the lack of suitable experimental data to validate the failure criteria in their completeness [33] as experimental set-up limit the achievable stress states. To overcome this issue, computational micromechanics was used to conduct virtual experiments, but since a complete validation is not possible, uncertainties for these stress states remained.

The limitation with fracture plane concepts for IFF prediction has led to the development of invariant-based failure criteria [14,15] which do not require the determination of the fracture plane orientation. Instead, a set of transversely isotropic invariants [34] is computed from the stress state and then used within a function that is at most quadratic in the stresses. The corresponding parameters of this failure function are obtained from the material strengths so that the failure index is equal to one at failure. This concept enables a quick assessment of stress states, which is more computationally efficient for full-scale structural simulations using, e.g., finite elements analysis. However, the calculation of the parameters, which depends on the choice of invariants for the failure function, can be problematic in the present invariant-based failure criteria. Since the failure envelope – implicitly defined by a failure index of one – must be convex, additional conditions on the material strengths [35] that might not meet the experimental data can occur, for example, for the failure criterion proposed by Camanho et al. [15]. Another point is that the number of parameters and thus the number of experimentally required material strengths must be kept minimal considering the limited experimental set-ups. Furthermore, a coupling of the tensile and compressive regime in the failure predictions, as employed by Christensen [14], is considered nonphysical [9]. Lastly, failure criteria, which rely on parameter determination using numerical optimization of non-convex functions [16], cannot be considered as suitable for a safety-relevant structural analysis because of ambiguous, respectively uncertain parameters as a mathematical–numerical consequence.

In essence, the main limitations of present failure criteria, which are addressed herein, are that (i) "(non-)interactive" failure criteria like Tsai–Wu [6], Tsai–Hill [5], or the maximum stress criterion [22] do not reflect the different failure modes present in FRPs [9]; (ii) fracture-plane based approaches [9,13] are computationally costly; (iii) failure criteria with parameters determined by numerical optimization [16] are not to be used; (iv) any failure criterion should limit the number of experiments necessary for calibration [36]; (v) coupling between tensile and compressive failure present in some failure criteria [14] must be avoided [9]; (vi) the mathematical formulation of a failure criterion must be robust w.r.t. material strengths obtained from the calibration experiments, so that it is has a non-negative Hessian for a wide range of materials, which is not necessarily given for present failure criteria [15].

The goal of this study was to develop novel invariant-based failure criteria, which address the above points of present invariant-based failure criteria, to predict failure of a unidirectional non-crimp fabric (UD-NCF) carbon fiber/epoxy composite material. The criteria distinguish between IFF, where linear and quadratic transversely isotropic stress-invariants were employed, and tensile or compressive FF modes, where the maximum stress criterion and an adapted kinking criterion have been utilized, respectively. For an assessment of the predictive capability, off-axis tensile and compression tests with the UD-NCF composite were performed and results compared to those predicted with the developed criteria as well as well-known criteria from the literature. The presented model addresses the above limitations, which serve as a guideline for the development of failure criteria for FRPs.

2. Notation

Generally, the developed failure criteria map a stress state to two scalar variables, the IFF index f_{M} and the FF index f_{F}, which are then reduced to a single scalar failure index $f : \mathbb{R}^6 \to \mathbb{R}$ by taking the maximum of the above values. A failure value f greater than one represents failure, i.e. a failed state must fulfill $f > 1$. Negative failure values only correspond to a not failed state and occur due to the nonlinear failure functions. The considered UD composite material exhibits transversely isotropic material behavior, i.e. the fiber direction is a preferred direction, which is denoted by the unit vector $\boldsymbol{a}$, and any rotation about this axis on the perpendicular plane does not change the material behavior. The components of the macroscopic, i.e. homogenized, stress tensor $\boldsymbol{\sigma}$ as well as of any other tensor resp. vector are given using a Cartesian coordinate system $\{\boldsymbol{e}_i\}$ of which the 1-axis shall coincide with global fiber direction $\boldsymbol{a}$ (material coordinate system). Only for the compressive FF mode, a micromechanical deviation of the fiber direction from the global direction $\boldsymbol{a}$ is considered. Values in differing (Cartesian) coordinate systems are denoted by the superscripts ψ, m, or m_0, respectively. In general, scalars are denoted by non-bold letters as f or X_{T}, vectors by bold, lower case letters as $\boldsymbol{a}$, and second order tensors by bold, upper case letters as $\boldsymbol{A}$. Matrices are denoted by double underlining as $\underline{\underline{a}}$. The second order identity tensor reads $\boldsymbol{I}$. A linear mapping of two second order tensors is symbolized by $\boldsymbol{AB}$ and the trace of a second order tensor is written as $\mathrm{tr}(\boldsymbol{A})$. The signum function $\mathrm{sgn}(\cdot)$ yields the sign of its argument. The compressive and tensile strengths are denoted by the upper case letter for the direction (x for the 1-axis, y for the 2- and 3-axis) and the respective index for compression or tension (i.e. $X_{\mathrm{C/T}}$ and $Y_{\mathrm{C/T}}$), and the shear strengths by S_{T} and S_{L} for transverse (in the 2-3-plane) and longitudinal (in the perpendicular planes) shear, respectively. The subscripts C and T referring to compressive and tensile values, respectively, also apply to the strength parameters α_i. The strengths are considered to be positive, i.e. the material fails under pure longitudinal compression $\sigma_{11} = -X_{\mathrm{C}}$. In combination with direct stresses as tension or compression, the terms longitudinal and transverse refer to the fiber direction and perpendicular directions, respectively.

3. Development of invariant-based failure criteria

3.1. General considerations

The developed failure criteria, which are derived within this section, consider three different intra-ply failure modes, namely IFF, tensile FF, and compressive FF. Thus, an IFF failure index, f_{M}, and the applicable FF failure index, f_{F}, must be calculated for the assessment of a stress state. In Sections 3.2 and 3.3, the invariant-based IFF function and the FF function are derived, which is followed by considerations for incorporating strain rate-dependency in Section 3.4.

3.2. Matrix failure (IFF)

Boehler [34] presents transversely isotropic invariants of the stress tensor,

$$\mathrm{tr}(\boldsymbol{\sigma}), \mathrm{tr}\left(\boldsymbol{\sigma}^2\right), \mathrm{tr}\left(\boldsymbol{\sigma}^3\right), \mathrm{tr}(\boldsymbol{A\sigma}), \mathrm{tr}\left(\boldsymbol{A\sigma}^2\right), \tag{1}$$

and an additive split of the stress tensor

$$\begin{aligned} \boldsymbol{\sigma}_{\mathrm{r}} &= \frac{1}{2}(\mathrm{tr}(\boldsymbol{\sigma}) - \mathrm{tr}(\boldsymbol{A\sigma}))\,\boldsymbol{I} - \frac{1}{2}(\mathrm{tr}(\boldsymbol{\sigma}) - 3\mathrm{tr}(\boldsymbol{A\sigma}))\,\boldsymbol{A} \\ \boldsymbol{\sigma}_{\mathrm{p}} &= \boldsymbol{\sigma} - \boldsymbol{\sigma}_{\mathrm{r}}. \end{aligned} \tag{2}$$

$\boldsymbol{A}$ denotes the second order tensor corresponding to the fiber direction, which is obtained by the dyadic product ($\otimes$) as $\boldsymbol{A} = \boldsymbol{a} \otimes \boldsymbol{a}$. Note, this is also the exact second order fiber orientation tensor for the given unidirectional microstructure, which can be obtained from the fiber orientation distribution function, Ψ, as $\boldsymbol{A} = \oint_S \boldsymbol{p} \otimes \boldsymbol{p}\Psi(\boldsymbol{p})\,\mathrm{d}p$ with the orientation $\boldsymbol{p} \in S = \left\{\boldsymbol{p} \in \mathbb{R}^3 \,|\, \|\boldsymbol{p}\| = 1\right\}$ and the conditions $\oint_S \Psi(\boldsymbol{p})\,\mathrm{d}p = 1$ and $\Psi(\boldsymbol{p}) = \Psi(-\boldsymbol{p}) \geq 0$ [37–39]. $\boldsymbol{\sigma}_{\mathrm{r}}$ is a superposition of the direct stress along the fiber direction and the average direct transverse stress and is also referred as reaction stress [15]. The remainder $\boldsymbol{\sigma}_{\mathrm{p}}$ is assumed to contribute to IFF and is also referred to as plasticity inducing stress by Camanho et al. [15].

Formulating the invariants in Eq. (1) in the stresses $\boldsymbol{\sigma}$ and $\boldsymbol{\sigma}_{\mathrm{p}}$ yields the transversely isotropic invariants as well as arbitrary linear combinations of them. This fact is used to create a set of invariants, which are linear or quadratic in the stresses, and a selection of the resulting invariants is chosen for a polynomial, invariant-based IFF function. Since it is assumed that IFF does not depend on longitudinal direct stresses, a suitable function can be composed of the following invariants

$$\begin{aligned} I_1 &= \mathrm{tr}\,(\boldsymbol{\sigma}) - \mathrm{tr}\,(\boldsymbol{A}\boldsymbol{\sigma}) \\ I_2 &= \mathrm{tr}\left(\boldsymbol{A}\boldsymbol{\sigma}_{\mathrm{p}}^2\right) \\ I_3 &= \mathrm{tr}\left(\boldsymbol{\sigma}^2\right) - \mathrm{tr}\left(\boldsymbol{A}\boldsymbol{\sigma}^2\right) - \mathrm{tr}\left(\boldsymbol{A}\boldsymbol{\sigma}_{\mathrm{p}}^2\right) \\ I_4 &= 2\mathrm{tr}\left(\boldsymbol{\sigma}_{\mathrm{p}}^2\right) - 4\mathrm{tr}\left(\boldsymbol{A}\boldsymbol{\sigma}_{\mathrm{p}}^2\right) \\ I_5 &= I_1^2 \\ I_6 &= \frac{I_4 - I_3}{2}, \end{aligned} \tag{3}$$

which can be written in terms of the stress tensor components

$$\begin{aligned} I_1 &= \sigma_{22} + \sigma_{33} \\ I_2 &= \sigma_{12}^2 + \sigma_{13}^2 \\ I_3 &= \sigma_{22}^2 + \sigma_{33}^2 + 2\sigma_{23}^2 \\ I_4 &= \left(\sigma_{22} - \sigma_{33}\right)^2 + 4\sigma_{23}^2 \\ I_5 &= \left(\sigma_{22} + \sigma_{33}\right)^2 \\ I_6 &= \sigma_{23}^2 - \sigma_{22}\sigma_{33} \end{aligned} \tag{4}$$

for $\boldsymbol{a} = \boldsymbol{e}_1$.

The objectives for choosing a set of the above invariants in Eq. (3) are a minimal number of required strength values, i.e. only the uniaxial strengths $Y_{\mathrm{C/T}}$ and $S_{\mathrm{L/T}}$, and (unconditionally) non-negative eigenvalues of the corresponding Hessian. The latter condition is necessary for failure criteria [40], whereas the former objective aims to minimize experimental testing or the nonphysical assumption of parameters where experimental data is not available, which might introduce uncertainties in the predictive capability [36]. The invariant-based criterion developed by Camanho et al. [15] requires additional biaxial or off-axis tests, which also limits the admissible combinations of strengths, and is for this reason not further discussed here. Another necessary condition for the IFF function is the occurrence of the longitudinal and transverse shear stresses as well as the transverse normal stress, which exhibits a tension/compression asymmetry. Thus, the IFF function must contain I_2 and at least one of the invariants I_3, I_4, or I_6.

Using the form

$$f_{\mathrm{M}} = \sum_i \alpha_i I_i \tag{5}$$

for the IFF function with the strength parameters α_i limits the number of invariants I_i to four if the required strengths are restricted to the ones mentioned above, since the parameters are obtained from a linear equation system resulting from $f_{\mathrm{M}} = 1$ for the uniaxial stress states with the above strengths. Another option is an additional distinction between matrix tension and compression based on the sign of I_1 as used by Hashin [8] or Camanho et al. [15]. This option reduces the number of invariants to three as there are two distinct sets of parameters $\alpha_{i\mathrm{C/T}}$, which need to be calculated from a linear equation system. Using three invariants and the described case distinction results in nine different and admissible combinations, namely 123, 124, 126, 234, 235, 236, 245, 246, and 256. For each of these combinations, the linear equation system resulting from $f_{\mathrm{M}} = 1$ is set up and solved, and the Hessian of the obtained IFF function is derived to evaluate the sign of its eigenvalues. For two combinations (123 and 124) the eigenvalues are unconditionally non-negative, one combination (126) is not admissible as it has one negative eigenvalue, and the remaining six combinations have only conditionally non-negative eigenvalues of the Hessian. Since the material parameters $X_{\mathrm{T}} = 1637$ MPa, $X_{\mathrm{C}} = 1001$ MPa, $Y_{\mathrm{T}} = 60$ MPa, $Y_{\mathrm{C}} = 179$ MPa, $S_{\mathrm{L}} = 90$ MPa, $S_{\mathrm{T}} = 80$ MPa for the investigated UD-NCF composite reported by Suratkar [41] or Rouf [42] yield at least one negative eigenvalue for the latter combinations, they are also not discussed in further details. Using four different invariants results for the combinations 1234, 1235, 1236, 1245, 1246, and 1256 in Christensen's IFF function [14] and the remaining combinations (2345, 2346, 2356, 2456) have at least one negative eigenvalue of the corresponding Hessian. Thus, the combinations of four different invariants are omitted here. The corresponding Hessians for the remaining combinations can be found in the Appendix. Hereafter, two new IFF failure criteria will be presented, namely the criteria based on the combinations 123 (I_{123}) and 124 (I_{124}) of the invariants in Eq. (3).

3.2.1. I_{123} failure criterion

As explained in Section 3.2, the IFF function of the new failure criterion named I_{123} reads as

$$f_{\mathrm{M}} = \alpha_1 I_1 + \alpha_2 I_2 + \alpha_3 I_3 \tag{6}$$

with

$$\begin{aligned} \alpha_1 &= \alpha_{1\mathrm{T}} && \text{if } I_1 > 0 \\ \alpha_1 &= \alpha_{1\mathrm{C}} && \text{if } I_1 \leq 0 \end{aligned} \tag{7}$$

and the invariants I_i as defined in Eq. (3). The linear equation system resulting from the conditions $f_{\mathrm{M}} = 1$ at the uniaxial strength values $Y_{\mathrm{C/T}}$ and $S_{\mathrm{T/L}}$ reads

$$\begin{aligned} Y_{\mathrm{C}}^2\alpha_3 - Y_{\mathrm{C}}\alpha_{1\mathrm{C}} &= 1 \\ Y_{\mathrm{T}}^2\alpha_3 + Y_{\mathrm{T}}\alpha_{1\mathrm{T}} &= 1 \\ 2S_{\mathrm{T}}^2\alpha_3 &= 1 \\ S_{\mathrm{L}}^2\alpha_2 &= 1 \end{aligned} \tag{8}$$

and the solution for the strength parameters $\alpha_{i\mathrm{C/T}}$ is

$$\begin{aligned} \alpha_{1\mathrm{T}} &= \frac{2S_{\mathrm{T}}^2 - Y_{\mathrm{T}}^2}{2S_{\mathrm{T}}^2 Y_{\mathrm{T}}} \\ \alpha_{1\mathrm{C}} &= -\frac{2S_{\mathrm{T}}^2 - Y_{\mathrm{C}}^2}{2S_{\mathrm{T}}^2 Y_{\mathrm{C}}} \\ \alpha_2 &= \frac{1}{S_{\mathrm{L}}^2} \\ \alpha_3 &= \frac{1}{2S_{\mathrm{T}}^2}. \end{aligned} \tag{9}$$

Since the strength parameters are positive (cf. Section 2), all eigenvalues are strictly positive (cf. Appendix) meeting the above mentioned condition. A reserve factor, i.e. a scaling factor for the current stress to failure, cannot be calculated directly with this formulation, since the function is neither linear nor quadratic in the stresses. An analytical reformulation to circumvent this issue is possible [9] but not done here. Due to the distinct parameter sets for transverse tension and compression, it is not ensured that all combinations of strengths are suitable, although all eigenvalues are strictly positive, as some combinations might lead to kinks in the failure surface (envelopes), which is implicitly defined by $f_{\mathrm{M}} = 1$. On the other hand, this distinction removes the coupling between these two load cases as postulated by Puck [9], which occurs for Christensen's IFF function.

3.2.2. I_{124} failure criterion

Analogously to Section 3.2.1, the IFF function for the I_{124} failure criterion reads as

$$f_{\mathrm{M}} = \alpha_1 I_1 + \alpha_2 I_2 + \alpha_4 I_4 \tag{10}$$

with

$$\alpha_1 = \alpha_{1\mathrm{T}} \quad \text{if } I_1 > 0$$
$$\alpha_1 = \alpha_{1\mathrm{C}} \quad \text{if } I_1 \leq 0 \tag{11}$$

and the invariants I_i as defined in Eq. (3). The strength parameters $\alpha_{i\mathrm{C/T}}$ are calculated from the linear equation system

$$\begin{aligned} Y_\mathrm{C}^2\alpha_4 - Y_\mathrm{C}\alpha_{1\mathrm{C}} &= 1 \\ Y_\mathrm{T}^2\alpha_4 + Y_\mathrm{T}\alpha_{1\mathrm{T}} &= 1 \\ 4S_\mathrm{T}^2\alpha_4 &= 1 \\ S_\mathrm{L}^2\alpha_2 &= 1 \end{aligned} \tag{12}$$

with the solution

$$\begin{aligned} \alpha_{1\mathrm{T}} &= \frac{4S_\mathrm{T}^2 - Y_\mathrm{T}^2}{4S_\mathrm{T}^2 Y_\mathrm{T}} \\ \alpha_{1\mathrm{C}} &= -\frac{4S_\mathrm{T}^2 - Y_\mathrm{C}^2}{4S_\mathrm{T}^2 Y_\mathrm{C}} \\ \alpha_2 &= \frac{1}{S_\mathrm{L}^2} \\ \alpha_4 &= \frac{1}{4S_\mathrm{T}^2}. \end{aligned} \tag{13}$$

Four eigenvalues of the respective Hessian are strictly positive due to the positive strengths and one eigenvalue is zero (cf. Appendix). Thus, there is a combination of non-zero stresses, which can be scaled infinitely, not leading to a prediction of failure. This combination is equi-biaxial transverse compression $\sigma_{22} = \sigma_{33} < 0$, because $I_4 = 0$ holds and $\alpha_{1\mathrm{C}} > 0$ in combination with $I_1 < 0$ results in $f_\mathrm{M} < 0$, which is considered as no failure. Regarding the reserve factor, the admissible strengths, and the decoupling of compression and tension, the same as in Section 3.2.1 applies.

3.3. Fiber failure (FF)

Christensen [14] derives a maximum stress criterion to assess the FF index, i.e.

$$f_\mathrm{F} = \frac{\sigma_{11}}{X_\mathrm{T}} \quad \text{for } \sigma_{11} \geq 0$$
$$f_\mathrm{F} = \frac{|\sigma_{11}|}{X_\mathrm{C}} \quad \text{for } \sigma_{11} < 0 \tag{14}$$

or expressed with invariants and tensor-notation

$$f_\mathrm{F} = \frac{\mathrm{tr}\,(\boldsymbol{A\sigma})}{X_\mathrm{T}} \quad \text{for } \mathrm{tr}\,(\boldsymbol{A\sigma}) \geq 0$$
$$f_\mathrm{F} = \frac{|\mathrm{tr}\,(\boldsymbol{A\sigma})|}{X_\mathrm{C}} \quad \text{for } \mathrm{tr}\,(\boldsymbol{A\sigma}) < 0. \tag{15}$$

Tensile FF is often evaluated using the maximum stress criterion [43], for instance by the Hashin-Rotem [3,4,7], the LaRC05 [13] or Camanho's invariant-based criterion [15], which is also considered here. However, compressive FF is known to occur due to fiber kinking [13,15,44,45], where the underlying mechanism is still topic of current research. Fiber kinking is reported to be sensitive to manufacturing defects such as voids or initial fiber misalignment [44]. Experimental data suggest an interaction between the longitudinal compressive and shear stress [46], which cannot be modeled using a maximum stress criterion. For this reason, kinking criteria are developed by various researchers [13,15,47–49]. Rosen [47] assumes that in-phase micro-buckling of the fibers leads to the formation of kink-bands, whereas Argon [48] assumes that matrix damage in the vicinity of fibers leads to reduced lateral fiber support and, thus, fiber kinking. Camanho et al. [15] and Pinho et al. [13] use the latter approach to assess the FF index where local matrix damage is assumed to initiate near initially misaligned fibers, which leads to local shearing stresses and instability. The same approach is adapted here.

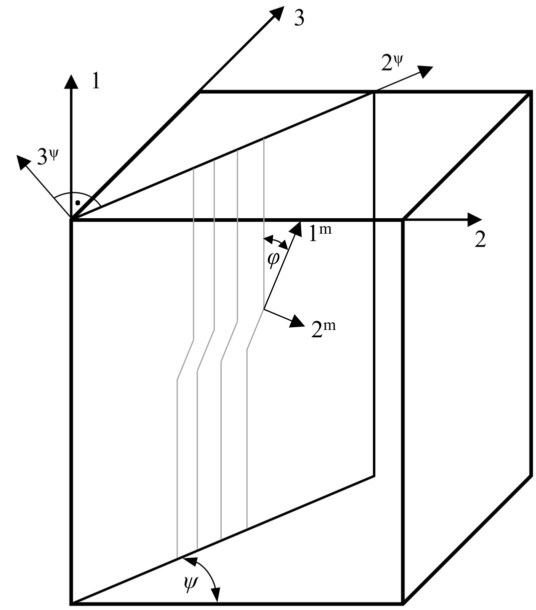

Fig. 1. Schematic of kinking plane and fiber misalignment angle for a UD composite.

Since the initial fiber misalignment generally depends on the manufacturing process, the geometry of the part, and the material system [43], it is not a material property. However, Pinho et al. [13] calculated the initial fiber misalignment from the longitudinal compressive strength to avoid the additional effort of measuring the misalignment angle. The orientation of the kinking plane is defined relative to the 1-2-plane by the kinking plane angle, ψ, where the respective coordinate system of the kinking plane is denoted by the superscript ψ (Fig. 1). In general, the kinking plane angle is dependent on the magnitude of the longitudinal compressive stress and the shear stress components and can be determined using an iterative approach [15]. The kinking angle (i.e., fiber misalignment angle), φ, can be seen on the kinking plane as a rotation of the corresponding coordinate system about the 3^ψ-axis to the misaligned frame which is denoted by the superscript m (or m_0 for the initially misaligned frame) as depicted in Figs. 1 and 2.

An additive split of the total fiber misalignment angle, φ

$$\varphi = \varphi_0 + \gamma_\mathrm{R} \tag{16}$$

into the initial fiber misalignment φ_0 (e.g., due to manufacturing defect) and a load-induced rotation γ_R

$$\gamma_\mathrm{R} = \gamma_{12}\left(\underline{\sigma}^{\mathrm{m}_0}\right), \tag{17}$$

due to the (shear) stress in the initially misaligned frame $\underline{\sigma}^{\mathrm{m}_0}$, is introduced to calculate the initial misalignment from the longitudinal compressive strength X_C. The material behavior in the misaligned frame is assumed to be transversely isotropic; thus, Eq. (17) can be reduced to

$$\gamma_\mathrm{R} = \gamma_{12}\left(\sigma_{12}^{\mathrm{m}_0}\right). \tag{18}$$

Assuming linear elastic (longitudinal) shear response, Eq. (18) can be simplified further to

$$\gamma_\mathrm{R} = \frac{\sigma_{12}^{\mathrm{m}_0}}{G_{12}}, \tag{19}$$

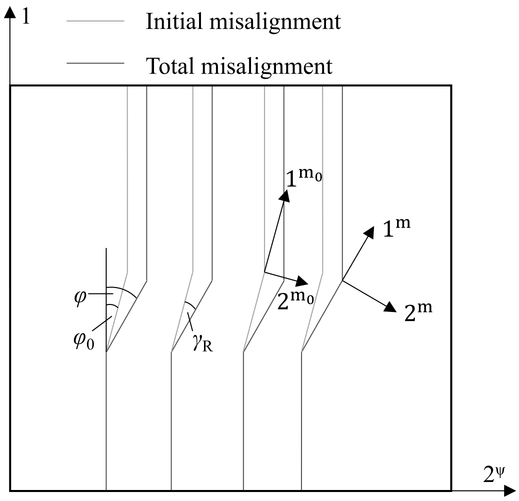

Fig. 2. Initial and total fiber misalignment angle for a UD composite.

where G_{12} denotes the longitudinal shear modulus of the UD composite. Using the transverse isotropy, the modification

$$\varphi = \operatorname{sgn}\left(\sigma_{12}^{\psi}\right)\varphi_0 + \gamma_\mathrm{R} \tag{20}$$

prevents a vanishing shear stress due to opposite signs [13].

The stress state $\underline{\sigma}^{\mathrm{m}_0}$ in the misaligned frame is obtained by the transformation according to

$$\underline{\sigma}^{\mathrm{m}_0} = \underline{\underline{Q}}\,\underline{\sigma}\,\underline{\underline{Q}}^\mathsf{T} \tag{21}$$

with the rotation matrix $\underline{\underline{Q}}$ in the standard base

$$Q_{ij} = \begin{pmatrix} 1 & 0 & 0 \\ 0 & \cos\psi & \sin\psi \\ 0 & -\sin\psi & \cos\psi \end{pmatrix} \tag{22}$$

and a subsequent rotation according to Eq. (21) with the rotation matrix in the standard base

$$Q_{ij} = \begin{pmatrix} \cos\varphi_0 & \sin\varphi_0 & 0 \\ -\sin\varphi_0 & \cos\varphi_0 & 0 \\ 0 & 0 & 1 \end{pmatrix}. \tag{23}$$

Since IFF in the misaligned frame is assumed to cause kinking [13], solving $f_\mathrm{M} = 1$ with the stress state

$$\sigma_{ij} = \begin{pmatrix} -X_\mathrm{C} & 0 & 0 \\ & 0 & 0 \\ \text{sym.} & & 0 \end{pmatrix} \tag{24}$$

in the global coordinate system $\{e_i\}$ and the misaligned fiber direction $\boldsymbol{a}$ [15]

$$a_i = \begin{pmatrix} \cos\varphi_\mathrm{c} \\ \cos\psi\sin\varphi_\mathrm{c} \\ \sin\psi\sin\varphi_\mathrm{c} \end{pmatrix} \tag{25}$$

yields the misalignment angle at failure under pure longitudinal compression φ_c

$$\varphi_\mathrm{c} = \frac{1}{2}\arccos\frac{-\alpha_3 X_\mathrm{C} + k + \alpha_{1\mathrm{C}}}{(\alpha_2 - \alpha_3)\,X_\mathrm{C}} \tag{26}$$

with

$$k = \sqrt{X_\mathrm{C}^2\alpha_2^2 - 2X_\mathrm{C}\alpha_{1\mathrm{C}}\alpha_2 + \alpha_{1\mathrm{C}}^2 - 4\alpha_2 + 4\alpha_3}. \tag{27}$$

The above equations hold for both, I_{123} and I_{124}, if α_3 is replaced by α_4 for the latter. The initial misalignment φ_0 can then be calculated as

$$\varphi_0 = \varphi_\mathrm{c} - \gamma_{12}\left(\frac{X_\mathrm{C}\sin 2\varphi_0}{2}\right), \tag{28}$$

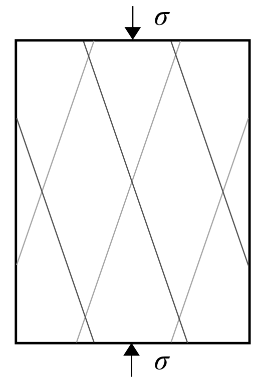

Fig. 3. Off-axis compression test.

using the additive split in Eq. (16) (or Eq. (20)), for a (potentially nonlinear) general longitudinal shear behavior $\gamma_{12} = \gamma_{12}(\sigma_{12})$. E.g. Newton's method can be used to solve the nonlinear Eq. (28) numerically. A small angles approximation and linear shear behavior allow an analytical solution of Eq. (28) for φ_0 as

$$\varphi_0 = \frac{\varphi_\mathrm{c}}{1 + \frac{X_\mathrm{C}}{G_{12}}}. \tag{29}$$

To calculate the FF index for a given stress state, the misalignment angle φ is determined according to Eq. (20) and then used to evaluate the IFF index in the misaligned frame defined by the kinking plane angle ψ and the misalignment angle φ. This done using Eq. (25) (with φ instead of φ_c) for the misaligned fiber direction $\boldsymbol{a}$ and the tensor formulation of the invariants in Eq. (3). Since the global Cartesian coordinate system may be chosen arbitrary (with the restriction regarding the 1-axis as mentioned in Section 2) and the kinking plane angle ψ is unknown beforehand, Pinho et al. [13] maximize the IFF index in ψ. The maximal IFF value is then taken as the FF index. This procedure also means that there is no preferred kinking plane but it only depends on the stress state and the strengths.

In order to reduce the computational effort, an approximation for the kinking plane angle ψ is introduced by Camanho et al. [15],

$$\begin{aligned} \psi &= \arctan\frac{\sigma_{13}}{\sigma_{12}} && \text{if } \sigma_{12} \neq 0 \\ \psi &= \frac{\pi}{2} && \text{if } \sigma_{12} = 0 \wedge \sigma_{13} \neq 0 \end{aligned} \tag{30}$$

or for vanishing longitudinal shear $\sigma_{12} = \sigma_{13} = 0$

$$\begin{aligned} \psi &= \frac{1}{2}\arctan\frac{2\sigma_{23}}{\sigma_{22} - \sigma_{33}} && \text{if } \sigma_{22} \neq \sigma_{33} \\ \psi &= \frac{\pi}{4} && \text{otherwise,} \end{aligned} \tag{31}$$

avoiding the numerical optimization, which would otherwise be necessary to maximize the IFF index in ψ because there is no analytical solution for general stress states. Eq. (30) is derived by maximizing the shear stress in the misaligned frame w.r.t. ψ and neglecting the transverse stress components. Neglecting the transverse stresses in Eq. (30) seems reasonable, since the transverse stresses only have a minor influence on the kinking plane angle compared to the longitudinal shear stresses [43].

A problem with this approximation is that the resulting shear stress $\sigma_{12}^{\mathrm{m}_0}$, and as a consequence the failure index, is sensitive to the sign of the shear stresses. For example, this can be demonstrated using an off-axis compression test as an example with the global uniaxial stress σ (Fig. 3). In the material coordinate system the stress state reads as

$$\sigma_{ij} = \sigma\begin{pmatrix} \cos^2\beta & \cos\beta\sin\beta & 0 \\ & \sin^2\beta & 0 \\ \text{sym.} & & 0 \end{pmatrix} \tag{32}$$

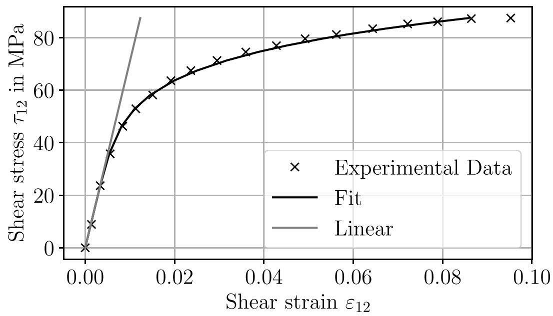

Fig. 4. Nonlinear shear stress–strain data of UD-NCF carbon fiber/epoxy composite material taken from Suratkar [41] and polynomial fit.

defined by the off-axis angle $|\beta| \leq \pi/2$. Eq. (32) shows that the chosen sign of β determines the sign of the shear stress. Although the resulting fiber orientations in the global coordinate system differ (light or dark gray in Fig. 3), the material behavior must not change, as Fig. 3 demonstrates. Applying the approximation in the Eqs. (30) yields a constant kinking plane angle $\psi = 0$ due to $\sigma_{13} = 0$ and $\arctan 0 = 0$. The shear stress in the misaligned frame results in

$$\sigma_{12}^{\mathrm{m}_0} = \frac{\sigma}{2}\left(-\cos^2\beta + \sin^2\beta\right)\sin 2\varphi_0 + \sigma\cos\beta\,|\sin\beta|\cos 2\varphi_0 \tag{33}$$

or

$$\sigma_{12}^{\mathrm{m}_0} = \frac{\sigma}{2}\left(-\cos^2\beta + \sin^2\beta\right)\sin 2\varphi_0 - \sigma\cos\beta\,|\sin\beta|\cos 2\varphi_0, \tag{34}$$

yielding different misalignment angles φ (for $\sigma \neq 0$; cf. Eq. (20)). Consequently different values for the invariants and the failure index are obtained contradicting the above postulation of similar failure indices. For stress states with at least one vanishing shear stress the material coordinate system can be rotated around the 1-axis (cf. Eqs. (21) and (22)) so that the signs of the remaining shear stresses are changed to maximize the shear stress $\sigma_{12}^{\mathrm{m}_0}$ and, thus, the failure index.

Regardless of the above issue, a Monte-Carlo simulation with 500,000 random stress states (with $\sigma_{11} < 0$ and positive shear stresses) showed that significant differences between the failure values obtained by the approximating formulae and an angle search (here defined as a difference in the failure indices greater than 0.03) only occur in approximately 1% of the compared cases. The approximation is considered reasonable given the computational effort otherwise required for the search to determine the kinking plane angle. A structured comparison shows that the approximation fails (among others) when the transverse and longitudinal shear stress is zero and transverse compression in 2-direction or transverse tension in 3-direction is acting. In these cases, the approximation in Eq. (31) yields $\psi = 0$, regardless of the transverse direct stresses, whereas the angle search results in $\psi = \pi/2$. According to this, transverse compression in the kinking plane impedes kinking, whereas tension promotes kinking. To incorporate this, Eq. (31) is modified to

$$\begin{aligned}
\psi &= \frac{1}{2}\arctan\frac{2\sigma_{23}}{\sigma_{22} - \sigma_{33}} && \text{if } \sigma_{22} \neq \sigma_{33} \wedge \sigma_{23} \neq 0 \\
\psi &= \frac{\pi}{2} && \text{if } \sigma_{23} = 0 \wedge \sigma_{33} > \sigma_{22} \\
\psi &= 0 && \text{if } \sigma_{23} = 0 \wedge \sigma_{22} > \sigma_{33} \\
\psi &= \frac{\pi}{4} && \text{otherwise.}
\end{aligned} \tag{35}$$

Although this might be an improvement for some stress states, the overall result of the Monte-Carlo simulation is remains consistent.

3.3.1. Nonlinear shear

The framework discussed above for compressive FF can capture the nonlinear shear response that is observed for UD-FRP [41,42,45,50–52]. For this purpose, a strain stress function $\gamma_{12} = \gamma_{12}(\sigma_{12})$ must be known and Eq. (28) must be solved numerically. Here, Newton's method is used with a starting value of zero for φ_0. The investigated material is modeled using an elasto-plastic constitutive model as described by Rouf [42]. For this reason, the stress strain relation $\sigma_{12} = \sigma_{12}(\gamma_{12})$ is known, but an inversion is computationally expensive. In order to assess the effect of the nonlinear shear behavior on the failure predictions, the quasi-static stress–strain relation reported by Suratkar [41] is approximated using a polynomial fit

$$\gamma_{12} = \frac{\sigma_{12}}{G_{12}} + 2c\sigma_{12}^{b}. \tag{36}$$

A least-squares estimation with fixed $G_{12} = 3550$ MPa [41] and $b = 6$ yields $c \approx 1.64 \cdot 10^{-13}$ MPa^{-6} and agreement with the experimental data (Fig. 4).

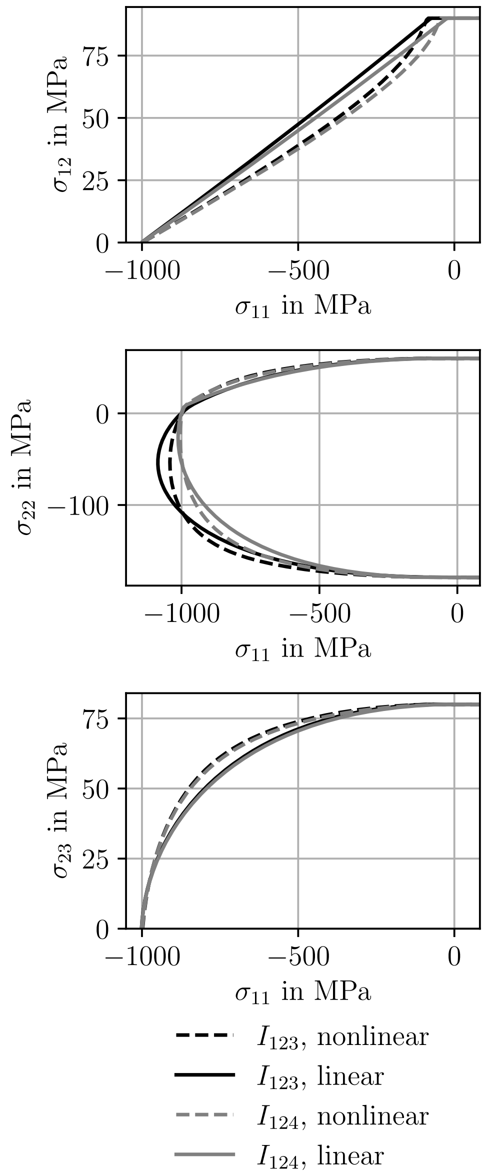

Fig. 5. Predicted failure envelopes using I_{123} and I_{124} for stress spaces with $\sigma_{11} < 0$. Comparison of predictions with linear and nonlinear shear behavior.

Fig. 5 compares the influence of the linear and nonlinear shear response on the failure criteria I_{123} and I_{124} using the shear response from Eq. (36) and the strengths in Table 1. As the nonlinear shear behavior effects only the kinking prediction, only the stress states with longitudinal compression are shown. Overall, there are relatively minor

Table 1
Uniaxial strengths for UD-NCF carbon fiber/epoxy composite material [41,53]. R_0 denotes the quasi-static value in MPa and m the coefficient for the strain rate dependency.

	X_T	X_C	Y_T	Y_C	S_L	S_T
R_0	1637	1001	60	179	90	80
m	0	0.06	0.04	0.09	0.1	0.1

Table 2
Quasi-static ($\dot{\varepsilon} = 0.003\ \mathrm{s}^{-1}$) uniaxial failure stresses in units of MPa for repeated off-axis tests, with mean and sample standard deviation (SD).

	Tension			Compression	
	15°	30°	45°	30°	45°
	237.2	126.9	77.6	182.6	184.2
	210.6	120.1	83.2	200.8	187.6
	278.4	123.2	79.5		
	250.8	121.8			
Mean	244.2	123.0	80.1	191.7	185.9
SD	28.2	2.9	2.8	12.9	2.4

differences with the predictions employing linear or nonlinear shear response, which is consistent with the results reported by Camanho et al. [15]. The discrepancies between predictions are slightly greater for stress states with compressive transverse stress, which was not the case when the transverse stress is tensile. The largest discrepancy was for the stress state with positive in-plane shear stress.

3.4. Strain rate dependency

Given that FRP materials exhibit strain rate-dependent behavior for certain deformation modes [16,29,42,43,52,54,55], the failure criteria were developed to account for this behavior. An empirical relation fitted to the experimental data can be used to describe the strain rate dependency of the material strengths. These functions can have, for instance, the general form

$$R\left(\dot{\varepsilon}\right) = R_0\left(1 + \sqrt{r\dot{\varepsilon}}\right) \tag{37}$$

with r defined as the fitting coefficient, R_0 denoting the quasi-static strength, and $\dot{\varepsilon}$ being a scalar (comparison) strain rate [43] or

$$R\left(\dot{\varepsilon}\right) = R_0\left(1 + m\log\frac{\dot{\varepsilon}}{\dot{\varepsilon}_0}\right) \tag{38}$$

using m as a coefficient to fit the data and $\dot{\varepsilon}_0$ as the reference strain rate taken from quasi-static tests [16]. Note, the reference strain rate is taken as $\dot{\varepsilon}_0 = 0.003\ \mathrm{s}^{-1}$ for all properties and the scaling factor is set to one for smaller comparison strain rates $\dot{\varepsilon}$, i.e. the above equation is only used for strain rates greater than the reference strain rate. The latter one is found to be an appropriate choice for the investigated material excluding the longitudinal tensile strength, which is considered as rate-independent [42,54]. The corresponding coefficients can be found in Table 1. For the longitudinal shear modulus G_{12}, the form in Eq. (38) is also used to describe the strain rate dependency. A quasi-static value of $G_{12} = 3400$ MPa and a corresponding coefficient $m = 0.02$ are used in the following sections. To reduce computational effort, a linear shear behavior is used hereafter. A simple polynomial fit as in Section 3.3.1 is not a reasonable approach as the stress strain relation for longitudinal shear is also strain rate-dependent. Thus, the necessary modification to incorporate the strain rate dependency is to implement the strain rate dependency of the strengths and the longitudinal shear modulus.

4. Experimental set-up and results

4.1. Material and manufacturing

The UD-NCF composite material considered in this study consisted of PX35 UD300 UD-NCF (Zoltek Corporation, US) [56] and a snap-curing three-part epoxy system (Westlake Epoxy) [57]. The NCF comprised UD tows, each with 50,000 continuous PX35 high strength carbon fibers, and transversely oriented supporting glass fibers, which were stitched in a tricot pattern with a polyester stitch. The resin system included EPIKOTE™ Resin TRAC 06150, EPIKURE™ Curing agent TRAC 06150 and an internal mold release agent HELOXY™ Additive TRAC 06805. Flat panels measuring 900 mm × 550 mm comprising either 8 or 11 aligned fabric layers of the material were manufactured using the high-pressure resin transfer molding (HP-RTM) process described in Cherniaev et al. [58]. The measured fiber volume fraction for the manufactured panels was approximately 53% [41], and void content was found to be less than 2% [54].

4.2. Experimental set-up

4.2.1. Specimens and set-up for compression tests

Specimens with nominal dimensions (length and width) of 10 mm × 10 mm and a thickness of 3.3 mm were cut from the manufactured panels using an abrasive water jet cutting machine. Specimens with shorter gauge lengths were chosen herein to avoid use of anti-buckling devices as they affect the system response due to friction. Also, anti-buckling devices cannot be used for high-rate dynamic tests because they impart inertial effects and cause undesired wave dispersions, which would inhibit dynamic stress equilibrium and, thus, render the test results meaningless. Short specimens have been used more frequently in recent years to capture the response of various material systems, including for composites [59–63] or sheet metals [64] (and the various references given therein), with samples up to one order of magnitude smaller. Scaling the specimen size (viz. cm and mm scale) has been shown to not change the material response [65]. Furthermore, a short specimen length is beneficial for Hopkinson bar experiments as the accuracy of the stress–strain data decreases with longer specimens [66]. Unidirectional off-axis specimens with a stacking sequence of $[30°]_{11}$ and $[45°]_{11}$ were subjected to a uniaxial compression load at room temperature to capture the axial stress at failure. Quasi-static tests were performed on a custom-built servo-hydraulic test frame equipped with an MTS 407 controller and a 90 kN capacity load cell under a uniaxial strain rate of 0.003 s^{-1}. High strain rate tests were performed on a compression split Hopkinson pressure bar (SHPB) apparatus with maraging steel bars under a uniaxial strain rate of 260 s^{-1}. The specimens were subjected to the end loading conditions for all tests performed. Further details about the test set-up can be found in Rouf et al. [53].

4.2.2. Specimens and set-up for tensile tests

Specimens with nominal dimensions (length and width) of 250 mm × 25 mm and a thickness of 2.6 mm. were cut from the manufactured panels using an abrasive water jet cutting machine. Unidirectional off-axis specimens with a stacking sequence of $[15°]_8$, $[30°]_8$, and $[45°]_8$ were subjected to a quasi-static uniaxial tensile load at room temperature. Aluminum end tabs matching the specimen width and 50 mm in length were bonded to the specimens using Loctite® 480 adhesive to prevent damage in the gripping region. Tests were performed in displacement control with a crosshead speed of 6 mm/min ($\dot{\varepsilon} = 0.003$ s^{-1}) using an MTS 45 Criterion electro–mechanical test frame equipped with a 100 kN capacity load cell. Specimens were gripped with a gripping pressure of 1500 psi. A black-and-white speckle pattern was applied, and photographs were recorded with a resolution of 2048 × 2048 pixels. Local displacement measurements and strain calculations were performed using digital image correlation (DIC) software (VIC-2D 7, Correlated Solutions) with a subset size of 31 pixels and a step

Table 3
Dynamic uniaxial compressive failure stresses in units of MPa for repeated off-axis tests performed at 260 s^{-1}, with mean and sample SD.

	30°	45°
	295.7	270.3
	275.3	250.0
	267.6	270.6
Mean	279.6	263.6
SD	14.5	11.8

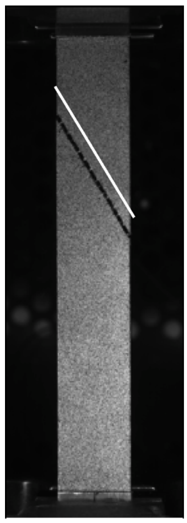

Fig. 6. A representative 30° off-axis tensile specimen with fracture in the gauge section. The white line indicates the fiber direction.

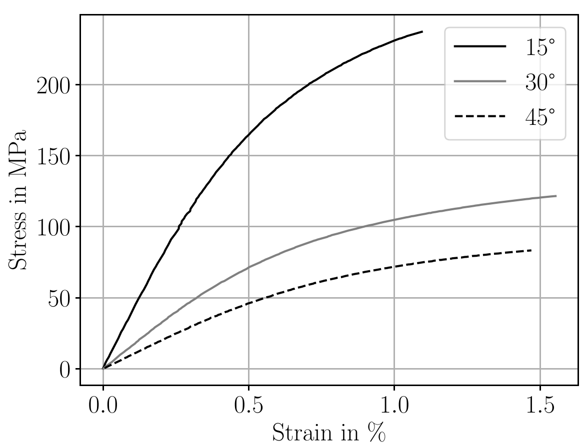

Fig. 7. Uniaxial stress–strain curves under quasi-static tensile loading.

size of 7 pixels. Test data, including the photographs, was recorded at 100 ms intervals and subsequently used to calculate the ultimate tensile strength. Further details about the test set-up can be found in Rouf et al. [53].

4.3. Experimental results

The tension and compression failure stresses obtained for the quasi-static off-axis tests are summarized in Table 2. Exemplary stress–strain curves for the quasi-static tensile tests for different off-axis angles are shown in Fig. 7. Fracture occurred for all tensile specimens parallel to the fiber direction (exemplarily shown for 30° off-axis in Fig. 6), indicating matrix failure. It should be noted that two out of the four

Table 4
Ratio of predicted quasi-static failure stress to mean experimental value for indicated off-axis specimens. Linear shear behavior was used for prediction of compressive failure stress.

Criterion	Tension			Compression	
	15°	30°	45°	30°	45°
I_{123}	1.25	1.16	1.17	1.09	0.98
I_{124}	1.23	1.14	1.15	0.96	0.87
Puck	1.25	1.16	1.17	1.46	1.27
LaRC05	1.26	1.16	1.15	1.32	1.19
Christensen	1.26	1.17	1.17	1.13	1.02
Hashin	1.37	1.28	1.25	1.07	0.89
Tsai–Wu	1.34	1.22	1.20	1.25	1.07
Max. Stress	1.47	1.69	1.50	1.08	0.97

Table 5
Ratio of predicted dynamic compressive failure stress to mean experimental value for indicated off-axis specimens. Linear shear behavior was used for predictions.

Criterion	30°	45°
I_{123}	1.08	1.00
I_{124}	0.96	0.90
Puck	1.51	1.32
LaRC05	1.34	1.23
Christensen	1.19	1.09
Hashin	1.08	0.92
Tsai–Wu	1.37	1.18
Max. Stress	1.11	1.02

15° off-axis tension specimens failed in the vicinity of the grip region (specimens 2 and 4 in Table 2); however, there seems to be no clear trend that indicates preliminary failure of these specimens, because the failure stresses of these specimens are the second and fourth highest obtained. Especially, considering the generally higher scatter in the present data prohibits the conclusion of a statistically significant deviation. Apart from the increased scatter for the 15° off-axis tensile specimens, a less pronounced scatter for the 30° off-axis compression tests is observed, whereas the other quasi-static tests show a very high repeatability. The compression failure stresses obtained at dynamic strain rate are presented in Table 3, which also shows that the scatter is notably increased compared to the quasi-static tests. Overall, the expected decrease in failure stress with increasing off-axis angle was observed for both strain rates, as well as the increase in failure stress for the dynamic tests.

5. Prediction results and discussion

5.1. Verification

Figs. 8, 9, and 10 display the failure envelopes for different stress spaces and three strain rates predicted using the I_{123} and I_{124} criteria using a linear shear behavior (cf. Section 3.4) and the corresponding uniaxial strengths. The uniaxial strengths are met for all envelopes at all strain rates, which is necessary for the verification. In Fig. 8 the strain rate independency of the longitudinal tensile strength can be observed. The remaining strengths are increased for higher strain rates as expectable from Eq. (38). Thus, the resulting envelopes for a particular stress space appear to be scaled up with increasing strain rate. The open envelope for the I_{124} criterion discussed in Section 3.2.2 for biaxial transverse compression can be verified (Fig. 9). Since the IFF functions of both failure criteria are reduced to the same terms if only shear stresses are acting, the failure envelopes in Fig. 10 must coincide. Also, the predicted envelopes for the I_{124} criteria are more conservative at all strain rates for combined compressive transverse and shear stresses (Fig. 9) as well as for combined compressive longitudinal and transverse stresses (Fig. 8).

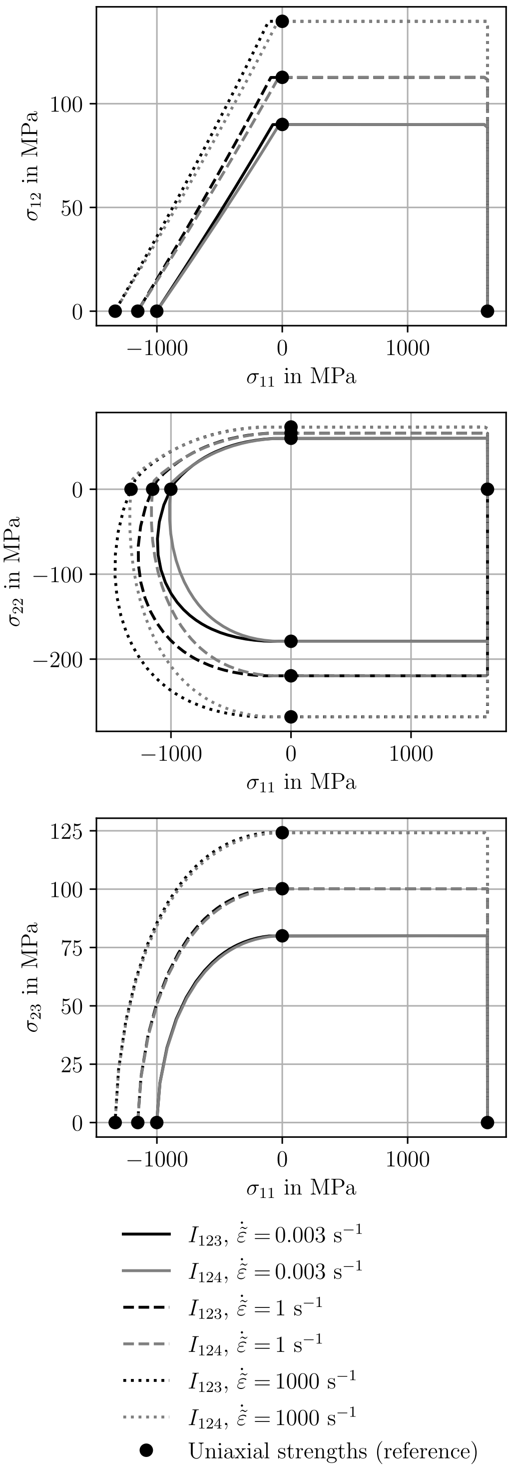

Fig. 8. Predicted failure envelopes for the I_{123} and I_{124} criteria at different strain rates: Longitudinal stresses.

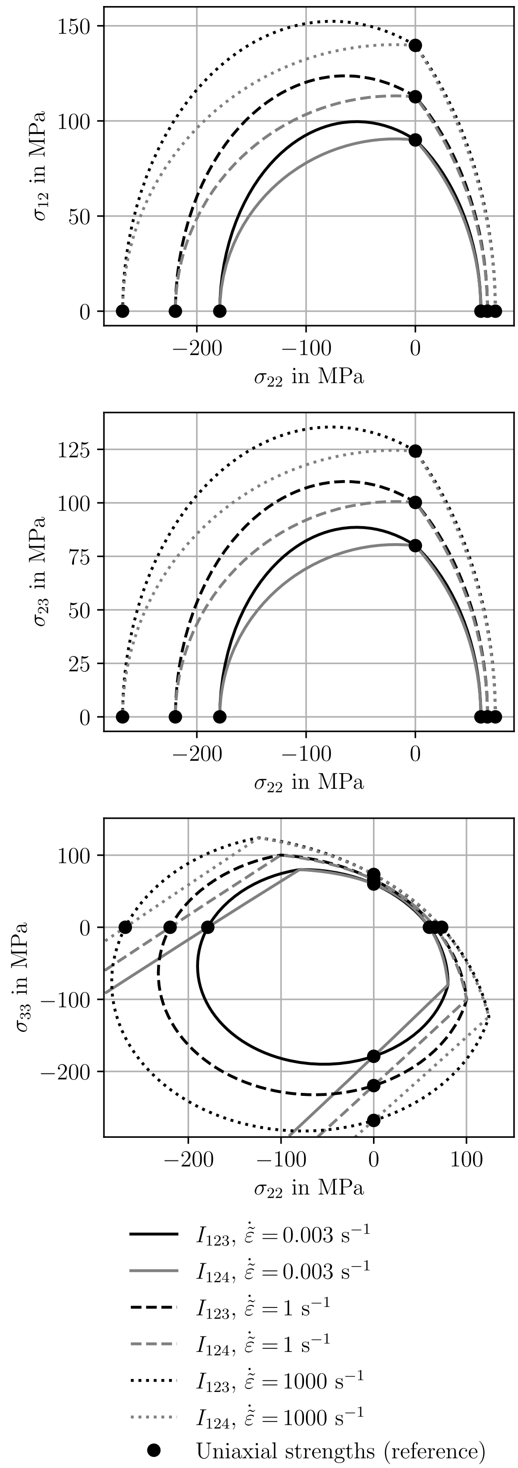

Fig. 9. Predicted failure envelopes for the I_{123} and I_{124} criteria at different strain rates: Transverse stresses.

5.2. Validation

The experimental results from the off-axis tests described in Section 4 are used for validation of the developed failure criteria. Table 4 shows the ratio of predicted over mean experimental failure stress for the quasi-static experiments on the off-axis specimens, where linear shear behavior was used for the prediction of the compressive failure stress. Use of nonlinear shear behavior reduces the ratio of I_{123} to 1.00 and 0.96 for the 30° and the 45° off-axis compression cases, respectively, while for I_{124} a reduction to 0.91 and 0.86 was predicted. Overall, the predicted failure stresses reasonably correlate with the experimental results, except for the 15° off-axis tension case where the deviation is greatest.

For comparison, Puck's [9,25,45], Christensen's [14], Hashin's [8] as well as the LaRC05 [13], Tsai–Wu [6], and maximum stress [22] criteria are included in Table 4. Christensen's compressive FF is originally a maximum stress criterion, but is replaced by a kinking criterion

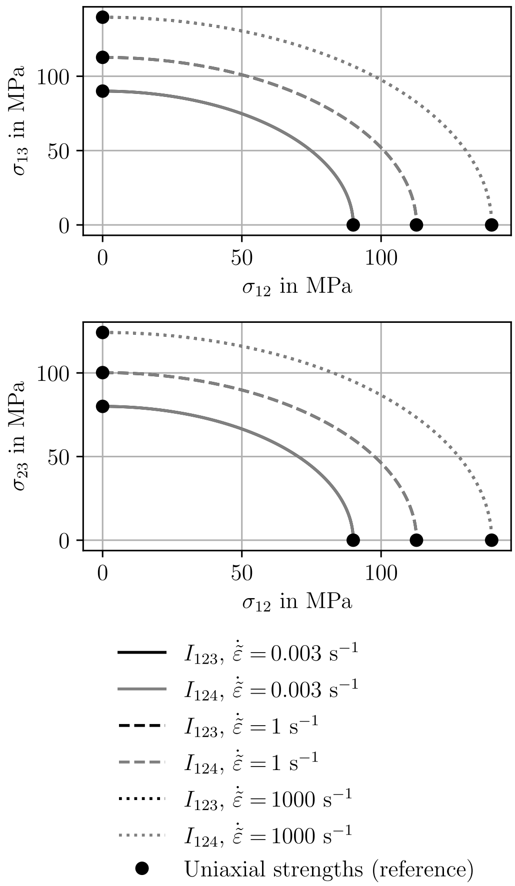

Fig. 10. Predicted failure envelopes for the I_{123} and I_{124} criteria at different strain rates: Shear stresses.

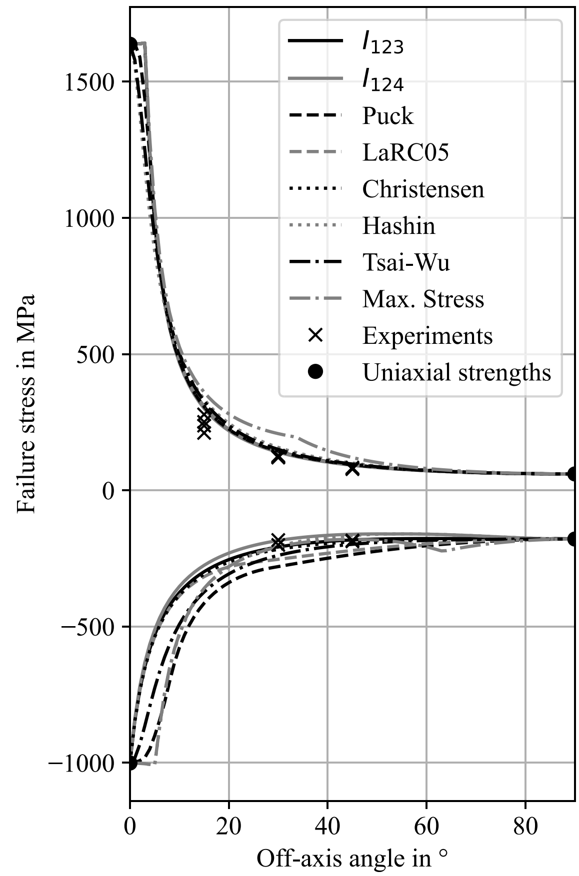

Fig. 11. Failure stress over off-axis angle predicted by the failure criteria and experimental values (quasi-static).

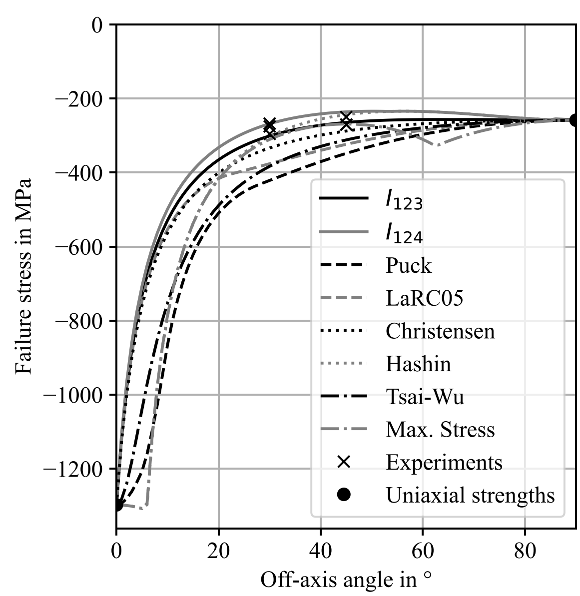

Fig. 12. Failure stress over off-axis angle predicted by the failure criteria and experimental values for a high strain rate ($\dot{\varepsilon} = 260$ s^{-1}).

here (similar as in Section 3.3). The obtained ratios for the tensile failure stresses are very similar to each other, except for the Hashin, Tsai–Wu and maximum stress criteria, with the failure stress overpredicted. The deviation for the Hashin, Tsai–Wu and maximum stress criteria is greater than for the other criteria, with the maximum stress criterion overpredicting the 30° off-axis tensile failure stress by 69% of the experimental value. The predicted compressive failure stress by criteria using a fracture plane approach deviated the most from the experimental data. A good predictive performance on the compressive failure is obtained from the proposed invariant-based criteria (I_{123} and I_{124}) as well as from Hashin's, Christensen's and the maximum stress failure criteria. Fig. 11 presents the maximum stress predictions for each criterion over a range of angles from 0° to 90°, showing a significant difference in compression between Puck, Tsai–Wu, and maximum stress and the remaining criteria for small off-axis angles as well as a difference between Puck and LaRC05 to the invariant-based criteria for intermediate off-axis angles. The former difference is owing to the different concept used by Puck for the compressive FF, while the latter difference caused by the more pronounced increase of the longitudinal shear strength under moderate transverse compression predicted by the fracture plane approach of Puck and LaRC05. The predicted maximum tensile stresses for the considered failure criteria are similar except for the maximum stress criterion, which shows a non-monotonic behavior causing a deviation at intermediate angles. This non-monotonic behavior of the maximum stress criterion can also be observed for large off-axis angles in compression. Apart from this, the trend of decreased failure stress with increased off-axis angle observed in the experiments can be reproduced with the exception that the invariant-based criteria predict a minimum in the failure stress at intermediate off-axis angles in compression, but this minimum is only slightly lower than the transverse compressive strength.

Analyzing the sensitivity of the failure stress prediction to the off-axis angle yields a change of about 22 MPa per degree for the 15°

Table 6
Used material properties in MPa as reported by Körber et al. [67].

X_T	X_C	Y_T	Y_C	S_L	S_T	G_{12}
2323	1017	62	255	90	62	5300

Table 7
Ratio of predicted quasi-static failure stress to mean experimental value for literature off-axis tensile specimens [55,67]. Linear shear behavior was used for prediction of compressive failure stress.

Criterion	Tension		
	15°	30°	45°
I_{123}	0.98	1.15	1.09
I_{124}	0.81	0.90	0.89
LaRC05	0.77	0.89	0.94
Christensen	0.81	0.90	0.88
Hashin	1.03	0.97	0.90
Tsai–Wu	0.93	0.94	0.89
Max. Stress	0.90	0.78	0.71

tensile test, whereas the sensitivity for the higher off-axis angles is reduced to a range of 1–5 MPa per degree (for tension and compression). This is also displayed in Fig. 11 and might contribute to the high scatter in the 15° experiments. Despite this, the agreement between the experiments and the prediction is excellent.

The comparison to the experimental results for the high strain rate can be found in Table 5 with linear shear used for the kinking criterion. The agreement between prediction and experiments is very good with a slight overprediction in compressive failure stress by I_{123} and underprediction by I_{124} (Fig. 12). Of the other failure criteria displayed for comparison, Hashin's criterion and the maximum stress criterion predict the obtained failure stresses best in the same range as I_{123} and I_{124}, while the remaining criteria overpredict failure to a larger extend, up to 51% in the case of Puck's failure criterion for the 30° off-axis test.

Moreover, the agreement with experimental data from the literature [55,67] for an UD IM7/8552 carbon fiber/epoxy composite is also found to be very good. The input properties are given in Table 6 and the comparison is shown in Tables 7 and 8, with a graphical representation given in Fig. 13. Overall, the results align well with the presented experimental evidence, and thus, the above explanations hold in a similar manner.

An additional advantage of the invariant-based approaches is that they allow an assessment of the stress state with minimal computational effort in contrast to the fracture plane approach, which requires numerical optimization to obtain the IFF index. To demonstrate this, the single core performance on a laptop CPU (13th Gen Intel Core i9-13900H, base speed 2.6 GHz) is shown in Table 9, which is obtained by the Python module *timeit* as mean execution time for 1000 different (random) stress states with 1000 calls each. Here, the times are normalized to the execution time of the I_{123} criterion and given with two significant digits. As it can be expected, the Hashin, Tsai–Wu and maximum stress criteria are the fastest since they require only a few arithmetic operations, followed by the invariant-based criteria that use the kinking criterion for longitudinal compression (with about a factor of 2.5). The criteria applying the fracture plane-concept are the slowest for evaluation, being more than one order of magnitude slower than the invariant-based criteria.

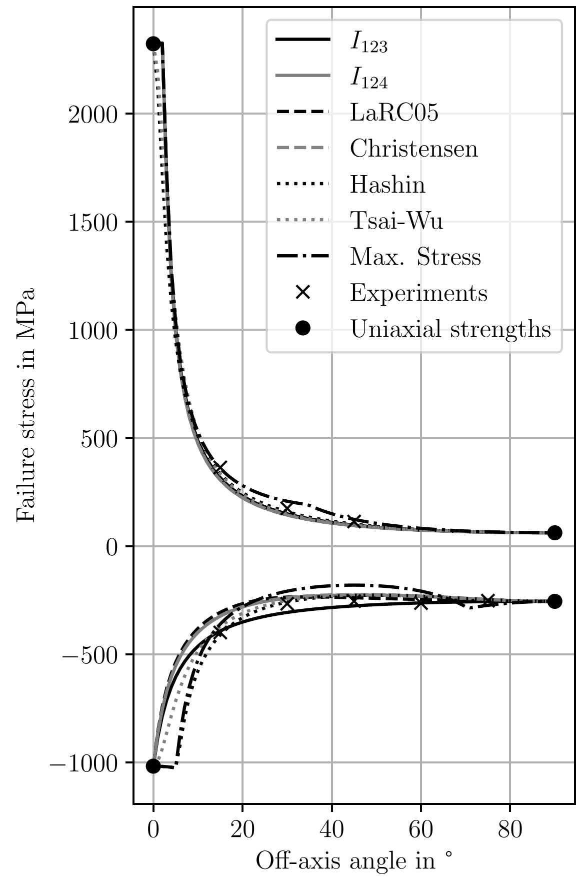

Fig. 13. Failure stress over off-axis angle predicted by the failure criteria and experimental values for UD IM7/8552 epoxy taken from [55,67].

Table 8
Ratio of predicted quasi-static failure stress to mean experimental value for literature off-axis compression specimens [55,67]. Linear shear behavior was used for prediction of compressive failure stress.

Criterion	Compression				
	15°	30°	45°	60°	75°
I_{123}	1.00	1.02	0.87	0.85	0.86
I_{124}	0.88	0.98	0.84	0.82	0.83
LaRC05	0.94	1.00	0.87	0.85	0.85
Christensen	0.87	0.98	0.84	0.82	0.83
Hashin	0.88	0.98	0.92	0.91	0.90
Tsai–Wu	0.88	0.98	0.92	0.86	0.86
Max. Stress	0.79	1.08	0.99	1.19	1.09

Table 9
Computational efficiency of the compared failure criteria.

Criterion	Relative time for evaluation
I_{123}	1
I_{124}	0.95
Puck	14
LaRC05	44
Christensen	1.01
Hashin	0.38
Tsai–Wu	0.40
Max. Stress	0.37

6. Conclusions

Two new failure criteria based on transversely isotropic invariants, namely I_{123} and I_{124}, have been developed to predict failure of a unidirectional non-crimp fabric (UD-NCF) carbon fiber/epoxy composite material. These criteria address the limitations of current failure criteria as identified herein and summarized hereafter. Different failure modes are considered as inter-fiber failure (IFF) and both compressive and tensile fiber failure (FF). The required experimental effort for calibration is kept to a minimum as only the uniaxial strengths of the material are considered. A distinction between matrix tension and compression decouples tensile and compressive behavior. This distinction can lead to kinks in the failure envelopes if an untypical combination of strengths is present, which was not the case for the considered material. On the contrary, it ensures non-negative eigenvalues of the Hessian as opposed to other present failure criteria in the literature. This invariant-based concept reduces computational effort when compared to well-known LaRC05 or Puck's criterion that utilize the fracture plane approach for inter-fiber failure (IFF). Furthermore, the new invariant-based criteria showed more accurate predictions for the off-axis compression tests performed with the UD-NCF carbon fiber/epoxy composite.

Strain rate dependency of the strengths was incorporated using an empirical relation and the nonlinear longitudinal shear response was considered as well for the fiber failure (FF) mode. Experiments performed at quasi-static and high strain rates were in good agreement with the predictions from the developed failure criteria. Experiments performed on specimens of the UD-NCF composite material system at quasi-static and high strain rates were in good agreement with the predictions from the developed failure criteria. The predictive capability of the criteria was also validated with experimental data for an UD tape composite material system. For both material systems, closed failure envelopes were ensured using the I_{123} criterion. Since the I_{124} criterion is often the more conservative choice of both, a combination of the presented failure criteria is a recommended approach for conservative predictions.

Future work will address use of tensorial strain rates, since the strain rate used in this study was a scalar comparison strain rate. Difficulties may arise from different longitudinal shear strain rates or transverse tensile/compressive strain rates. Another point is to consider the initial fiber misalignment for tensile FF mode as the sensitivity to misalignment is relatively high for longitudinal or off-axis tensile loading (at small off-axis angles). Moreover, the determination of the kinking plane should be investigated further to eliminate the sensitivity to the sign of the shear stresses, which would be of interest if there are preferred kinking planes due to the material microstructure, i.e., initial in-plane misalignment and out-of-plane crimping in UD-NCF composites.

CRediT authorship contribution statement

Nils Koltzenburg: Writing – original draft, Visualization, Methodology, Investigation, Formal analysis. **Khizar Rouf:** Writing – original draft, Visualization, Methodology, Investigation, Formal analysis. **Thomas Böhlke:** Writing – review & editing, Supervision, Funding acquisition. **John Montesano:** Writing – review & editing, Validation, Supervision, Resources, Project administration, Funding acquisition, Conceptualization.

Declaration of competing interest

The authors declare that they have no known competing financial interests or personal relationships that could have appeared to influence the work reported in this paper.

Acknowledgments

This study was funded by the Natural Sciences and Engineering Research Council of Canada (NSERC) through CRD Grant No. CRDPJ 507776-16 and Alliance Grant No. ALLRP 580246-22, the Ontario Advanced Manufacturing Consortium, Honda Research Institute US, Westlake Epoxy, Zoltek Corp. and Laval. NK and TB gratefully acknowledge the financial support by the German Research Foundation (DFG), project number 255730231, within the International Research Training Group "Integrated engineering of continuous–discontinuous long fiber reinforced polymer structures" (GRK 2078).

Appendix. Hessian matrices

I_{123} *failure criterion*

The matrix failure function for the I_{123} criterion

$$f_{\mathrm{M}} = \alpha_1 I_1 + \alpha_2 I_2 + \alpha_3 I_3 \tag{A.1}$$

with

$$\begin{aligned} I_1 &= \sigma_{22} + \sigma_{33} \\ I_2 &= \sigma_{12}^2 + \sigma_{13}^2 \\ I_3 &= \sigma_{22}^2 + \sigma_{33}^2 + 2\sigma_{23}^2 \end{aligned} \tag{A.2}$$

can be differentiated w.r.t. the stresses $\sigma_{22}, \sigma_{33}, \sigma_{23}, \sigma_{13}$, and σ_{12} yielding the Hessian in a standard base for the above stresses as

$$H_{f_{\mathrm{M}}} = \begin{pmatrix} 2\alpha_3 & 0 & 0 & 0 & 0 \\ & 2\alpha_3 & 0 & 0 & 0 \\ & & 4\alpha_3 & 0 & 0 \\ & & & 2\alpha_2 & 0 \\ \text{sym.} & & & & 2\alpha_2 \end{pmatrix} \tag{A.3}$$

containing only the eigenvalues

$$\begin{pmatrix} 2\alpha_2 & 2\alpha_2 & 2\alpha_3 & 2\alpha_3 & 4\alpha_3 \end{pmatrix}^{\mathsf{T}} \tag{A.4}$$

on its diagonal.

I_{124} *failure criterion*

The matrix failure function for the I_{124} criterion is

$$f_{\mathrm{M}} = \alpha_1 I_1 + \alpha_2 I_2 + \alpha_4 I_4 \tag{A.5}$$

with

$$\begin{aligned} I_1 &= \sigma_{22} + \sigma_{33} \\ I_2 &= \sigma_{12}^2 + \sigma_{13}^2 \\ I_4 &= \left(\sigma_{22} - \sigma_{33}\right)^2 + 4\sigma_{23}^2. \end{aligned} \tag{A.6}$$

The Hessian then reads in the above standard base as

$$H_{f_{\mathrm{M}}} = \begin{pmatrix} 2\alpha_4 & -2\alpha_4 & 0 & 0 & 0 \\ & 2\alpha_4 & 0 & 0 & 0 \\ & & 8\alpha_4 & 0 & 0 \\ & & & 2\alpha_2 & 0 \\ \text{sym.} & & & & 2\alpha_2 \end{pmatrix} \tag{A.7}$$

with the eigenvalues

$$\begin{pmatrix} 0 & 2\alpha_2 & 2\alpha_2 & 4\alpha_4 & 8\alpha_4 \end{pmatrix}^{\mathsf{T}}. \tag{A.8}$$

Data availability

Data will be made available on request.

References

[1] P. Gopal Samy Dharmaraj, Development of a Non-Crimp Fabric Carbon Fiber/epoxy Composite Technology Demonstrator (Master's thesis), University of Waterloo, Canada, 2020.

[2] M. Uustalu, Crush Simulation of Carbon/epoxy NCF Composites-Development of a Validation Test for Material Models (Master's thesis), KTH Royal Institute of Technology, Sweden, 2015.

[3] A. Puck, W. Schneider, On failure mechanisms and failure criteria of filament-wound glass-fibre/resin composites, Plast. Polym. 37 (127) (1969) 33–43.

[4] A. Puck, Festigkeitsberechnung an Glasfaser/Kunststoff-Laminaten bei zusammengesetzter Beanspruchung, Kunststoffe 59 (11) (1969) 780–787.

[5] V.D. Azzi, S.W. Tsai, Anisotropic strength of composites, Exp. Mech. 5 (9) (1965) 283–288, http://dx.doi.org/10.1007/BF02326292.

[6] S.W. Tsai, E.M. Wu, A general theory of strength for anisotropic materials, J. Compos. Mater. 5 (1) (1971) 58–80, http://dx.doi.org/10.1177/002199837100500106.

[7] Z. Hashin, A. Rotem, A fatigue failure criterion for fiber reinforced materials, J. Compos. Mater. 7 (4) (1973) 448–464, http://dx.doi.org/10.1177/002199837300700404.

[8] Z. Hashin, Fatigue failure criteria for unidirectional fiber composites, J. Appl. Mech. 47 (4) (1980) 329–334, http://dx.doi.org/10.1115/1.3153664.

[9] A. Puck, Festigkeitsanalyse von Faser-Matrix-Laminaten: Modelle für die Praxis, Carl Hanser Verlag, München, 1996.

[10] C.T. Sun, B.J. Quinn, J. Tao, D.W. Oplinger, Comparative Evaluation of Failure Analysis Methods for Composite Laminates (Final Report), Technical Report, DOT/FAA/AR-95/109, 1996.

[11] T.A. Bogetti, C.P.R. Hoppel, V.M. Harik, J.F. Newill, B.P. Burns, Predicting the nonlinear response and progressive failure of composite laminates, in: Failure Criteria in Fibre-Reinforced-Polymer Composites, Elsevier, 2004, pp. 402–428, http://dx.doi.org/10.1016/b978-008044475-8/50017-2.

[12] R.G. Cuntze, A. Freund, The predictive capability of failure mode concept-based strength criteria for multidirectional laminates, Compos. Sci. Technol. 64 (3–4) (2004) 343–377, http://dx.doi.org/10.1016/S0266-3538(03)00218-5.

[13] S.T. Pinho, R. Darvizeh, P. Robinson, C. Schuecker, P.P. Camanho, Material and structural response of polymer-matrix fibre-reinforced composites, J. Compos. Mater. 46 (19–20) (2012) 2313–2341, http://dx.doi.org/10.1177/0021998312454478.

[14] R.M. Christensen, The Theory of Materials Failure, Oxford University Press, Oxford, 2013.

[15] P.P. Camanho, A. Arteiro, A.R. Melro, G. Catalanotti, M. Vogler, Three-dimensional invariant-based failure criteria for fibre-reinforced composites, Int. J. Solids Struct. 55 (2015) 92–107, http://dx.doi.org/10.1016/j.ijsolstr.2014.03.038.

[16] I.M. Daniel, S.M. Daniel, J.S. Fenner, A new yield and failure theory for composite materials under static and dynamic loading, Int. J. Solids Struct. 148–149 (2018) 79–93, http://dx.doi.org/10.1016/j.ijsolstr.2017.08.036.

[17] A.S. Kaddour, M.J.K.A. Hinton, Benchmarking of triaxial failure criteria for composite laminates: Comparison between models of Part A of WWFE-II, J. Compos. Mater. 46 (19–20) (2012) 2595–2634, http://dx.doi.org/10.1177/0021998312449887.

[18] J. Görthofer, M. Schneider, A. Hrymak, T. Böhlke, A convex anisotropic damage model based on the compliance tensor, Int. J. Damage Mech. 31 (1) (2022) 43–86, http://dx.doi.org/10.1177/10567895211019065.

[19] P.A. Hessman, F. Welschinger, K. Hornberger, T. Böhlke, A micromechanical cyclic damage model for high cycle fatigue failure of short fiber reinforced composites, Compos. B 264 (2023) 110855, http://dx.doi.org/10.1016/j.compositesb.2023.110855.

[20] M. Schemmann, J. Görthofer, T. Seelig, A. Hrymak, T. Böhlke, Anisotropic mean-field modeling of debonding and matrix damage in SMC composites, Compos. Sci. Technol. 161 (2018) 143–158, http://dx.doi.org/10.1016/J.COMPSCITECH.2018.03.041.

[21] A.S. Kaddour, M.J.K.A. Hinton, P.A. Smith, S. Li, The background to the third world-wide failure exercise, J. Compos. Mater. 47 (20–21) (2013) 2417–2426, http://dx.doi.org/10.1177/0021998313499475.

[22] P.A. Zinoviev, S.V. Grigoriev, O.V. Lebedeva, L.P. Tairova, The strength of multilayered composites under a plane-stress state, Compos. Sci. Technol. 58 (7) (1998) 1209–1223, http://dx.doi.org/10.1016/S0266-3538(97)00191-7.

[23] J. Deng, Z. Hong, Q. Yin, T.J. Lu, A physically-based failure analysis framework for fiber-reinforced composite laminates under multiaxial loading, Compos. Struct. 241 (2020) 112125, http://dx.doi.org/10.1016/j.compstruct.2020.112125.

[24] J. Hund, C. Leppin, T. Böhlke, J. Rothe, Stress-strain characterization and damage modeling of glass-fiber-reinforced polymer composites with vinylester matrix, J. Compos. Mater. 51 (4) (2017) 547–562, http://dx.doi.org/10.1177/0021998316648227.

[25] A. Puck, H. Schürmann, Failure analysis of FRP laminates by means of physically based phenomenological models, Compos. Sci. Technol. 58 (7) (1998) 1045–1067, http://dx.doi.org/10.1016/S0266-3538(96)00140-6.

[26] Verein Deutscher Ingenieure, VDI 2014 Blatt 3–Entwicklung von Bauteilen aus Faser-Kunststoff-Verbund; Berechnungen, 2006.

[27] J. Wiegand, N. Petrinic, B. Elliott, An algorithm for determination of the fracture angle for the three-dimensional Puck matrix failure criterion for UD composites, Compos. Sci. Technol. 68 (12) (2008) 2511–2517, http://dx.doi.org/10.1016/j.compscitech.2008.05.004.

[28] F.J. Schirmaier, J. Weiland, L. Kärger, F. Henning, A new efficient and reliable algorithm to determine the fracture angle for Puck's 3D matrix failure criterion for UD composites, Compos. Sci. Technol. 100 (2014) 19–25, http://dx.doi.org/10.1016/j.compscitech.2014.05.033.

[29] D.M. Thomson, H. Cui, B. Erice, J. Hoffmann, J. Wiegand, N. Petrinic, Experimental and numerical study of strain-rate effects on the IFF fracture angle using a new efficient implementation of Puck's criterion, Compos. Struct. 181 (2017) 325–335, http://dx.doi.org/10.1016/j.compstruct.2017.08.084.

[30] M.J.K.A. Hinton, A.S. Kaddour, P.D. Soden, Failure Criteria in Fibre Reinforced Polymer Composites: The World-Wide Failure Exercise, Elsevier, Amsterdam and London, 2004.

[31] M.J.K.A. Hinton, A.S. Kaddour, The background to the second world-wide failure exercise, J. Compos. Mater. 46 (19–20) (2012) 2283–2294, http://dx.doi.org/10.1177/0021998312449885.

[32] M.J.K.A. Hinton, A.S. Kaddour, The background to Part B of the second world-wide failure exercise: Evaluation of theories for predicting failure in polymer composite laminates under three-dimensional states of stress, J. Compos. Mater. 47 (6–7) (2013) 643–652, http://dx.doi.org/10.1177/0021998312473346.

[33] P.D. Soden, A.S. Kaddour, M.J.K.A. Hinton, Recommendations for designers and researchers resulting from the world-wide failure exercise, in: Failure Criteria in Fibre-Reinforced-Polymer Composites, Elsevier, 2004, pp. 1223–1251, http://dx.doi.org/10.1016/b978-008044475-8/50039-1.

[34] J.-P. Boehler (Ed.), Applications of Tensor Functions in Solid Mechanics, in: CISM Courses and Lectures, No. 292, Springer, Wien and New York, 1987, http://dx.doi.org/10.1007/978-3-7091-2810-7.

[35] R.M. Christensen, Completion and closure on failure criteria for unidirectional fiber composite materials, J. Appl. Mech. 81 (1) (2014) http://dx.doi.org/10.1115/1.4025177.

[36] A.S. Kaddour, M.J.K.A. Hinton, Maturity of 3D failure criteria for fibre-reinforced composites: Comparison between theories and experiments: Part B of WWFE-II, J. Compos. Mater. 47 (6–7) (2013) 925–966, http://dx.doi.org/10.1177/0021998313478710.

[37] S.G. Advani, C.L. Tucker III, The use of tensors to describe and predict fiber orientation in short fiber composites, J. Rheol. 31 (8) (1987) 751–784, http://dx.doi.org/10.1122/1.549945.

[38] P.A. Hessman, T. Riedel, F. Welschinger, K. Hornberger, T. Böhlke, Microstructural analysis of short glass fiber reinforced thermoplastics based on x-ray micro-computed tomography, Compos. Sci. Technol. 183 (2019) 107752, http://dx.doi.org/10.1016/j.compscitech.2019.107752.

[39] P.A. Hessman, F. Welschinger, K. Hornberger, T. Böhlke, On mean field homogenization schemes for short fiber reinforced composites: Unified formulation, application and benchmark, Int. J. Solids Struct. 230 (2021) 111141, http://dx.doi.org/10.1016/j.ijsolstr.2021.111141.

[40] K.-S. Liu, S.W. Tsai, A progressive quadratic failure criterion for a laminate, Compos. Sci. Technol. 58 (7) (1998) 1023–1032, http://dx.doi.org/10.1016/S0266-3538(96)00141-8.

[41] A.P. Suratkar, Damage in Non-Crimp Fabric Carbon Fiber Reinforced Epoxy Composites Under Various Mechanical Loading Conditions (Electronic Thesis and Dissertation Repository), The University of Western Ontario, 2022, 8731.

[42] K. Rouf, Characterizing and Modelling the Strain Rate-Dependent Constitutive Response of a Unidirectional Non-Crimp Fabric Composite Material (Ph.D. thesis), University of Waterloo, 2023.

[43] J. Wiegand, Constitutive Modelling of Composite Materials Under Impact Loading (Ph.D. thesis), Oxford University, UK, 2009.

[44] Q. Sun, H. Guo, G. Zhou, Z. Meng, Z. Chen, H. Kang, S. Keten, X. Su, Experimental and computational analysis of failure mechanisms in unidirectional carbon fiber reinforced polymer laminates under longitudinal compression loading, Compos. Struct. 203 (2018) 335–348, http://dx.doi.org/10.1016/j.compstruct.2018.06.028.

[45] H. Schürmann, Konstruieren mit Faser-Kunststoff-Verbunden, 2nd ed., in: VDI-Buch, Springer Berlin Heidelberg, Berlin, Heidelberg, 2007, 2., bearb. u. erw. Aufl.

[46] P.M. Jelf, N.A. Fleck, The failure of composite tubes due to combined compression and torsion, J. Mater. Sci. 29 (11) (1994) 3080–3084, http://dx.doi.org/10.1007/BF01117623.

[47] B.W. Rosen, Mechanics of composite strengthening, in: Fiber Composite Materials, American Society for Metals, 1965, pp. 37–75.

[48] A.S. Argon, Fracture of composites, Treatise Mater. Sci. Technol. 1 (1972) 79–114.

[49] E. Edge, Stress-based grant–sanders method for predicting failure of composite laminates, Compos. Sci. Technol. 58 (7) (1998) 1033–1041, http://dx.doi.org/10.1016/S0266-3538(96)00139-X.

[50] T. Vogler, S. Kyriakides, Inelastic behavior of an AS4/PEEK composite under combined transverse compression and shear. Part I: Experiments, Int. J. Plast. 15 (8) (1999) 783–806, http://dx.doi.org/10.1016/S0749-6419(99)00011-X.

[51] P.D. Soden, M.J. Hinton, A.S. Kaddour, Biaxial test results for strength and deformation of a range of E-glass and carbon fibre reinforced composite laminates: Failure exercise benchmark data, Compos. Sci. Technol. 62 (12–13) (2002) 1489–1514, http://dx.doi.org/10.1016/S0266-3538(02)00093-3.

[52] K. Rouf, M.J. Worswick, J. Montesano, Experimentally verified dual-scale modelling framework for predicting the strain rate-dependent nonlinear anisotropic deformation response of unidirectional non-crimp fabric composites, Compos. Struct. 303 (2023) 116384, http://dx.doi.org/10.1016/j.compstruct.2022.116384.

[53] K. Rouf, M. Worswick, J. Montesano, Effect of strain rate on the in-plane orthotropic constitutive response and failure behaviour of a unidirectional non-crimp fabric composite, Compos. A 181 (2024) 108166, http://dx.doi.org/10.1016/j.compositesa.2024.108166.

[54] K. Rouf, A. Suratkar, J. Imbert-Boyd, J. Wood, M.J. Worswick, J. Montesano, Effect of strain rate on the transverse tension and compression behavior of a unidirectional non-crimp fabric carbon fiber/snap-cure epoxy composite, Materials 14 (23) (2021) 7314, http://dx.doi.org/10.3390/ma14237314.

[55] H. Körber, J. Xavier, P.P. Camanho, High strain rate characterisation of unidirectional carbon-epoxy IM7-8552 in transverse compression and in-plane shear using digital image correlation, Mech. Mater. 42 (11) (2010) 1004–1019, http://dx.doi.org/10.1016/j.mechmat.2010.09.003.

[56] M. Ghazimoradi, E.A. Trejo, V. Carvelli, C. Butcher, J. Montesano, Deformation characteristics and formability of a tricot-stitched carbon fiber unidirectional non-crimp fabric, Compos. A 145 (2021) 106366, http://dx.doi.org/10.1016/j.compositesa.2021.106366.

[57] Y. Zeng, D. Cronin, J. Montesano, Characterization of the strain rate-dependent deformation response and fracture behaviour of a three-part snap-cure epoxy resin under tension and compression loading, J. Dyn. Behav. Mater. (2024) 1–18, http://dx.doi.org/10.1007/s40870-024-00419-9.

[58] A. Cherniaev, Y. Zeng, D. Cronin, J. Montesano, Quasi-static and dynamic characterization of unidirectional non-crimp carbon fiber fabric composites processed by HP-RTM, Polym. Test. 76 (2019) 365–375, http://dx.doi.org/10.1016/j.polymertesting.2019.03.036.

[59] H. Koerber, J. Xavier, P.P. Camanho, Y.E. Essa, F.M.D.L. Escalera, High strain rate behaviour of 5-harness-satin weave fabric carbon–epoxy composite under compression and combined compression–shear loading, Int. J. Solids Struct. 54 (2015) 172–182, http://dx.doi.org/10.1016/J.IJSOLSTR.2014.10.018.

[60] R.O. Ochola, K. Marcus, G.N. Nurick, T. Franz, Mechanical behaviour of glass and carbon fibre reinforced composites at varying strain rates, Compos. Struct. 63 (2004) 455–467, http://dx.doi.org/10.1016/S0263-8223(03)00194-6.

[61] K. Naresh, K. Shankar, B.S. Rao, R. Velmurugan, Effect of high strain rate on glass/carbon/hybrid fiber reinforced epoxy laminated composites, Compos. B 100 (2016) 125–135, http://dx.doi.org/10.1016/J.COMPOSITESB.2016.06.007.

[62] N.K. Naik, V.R. Kavala, High strain rate behavior of woven fabric composites under compressive loading, Mater. Sci. Eng.: A 474 (2008) 301–311, http://dx.doi.org/10.1016/J.MSEA.2007.05.032.

[63] J. Shim, D. Mohr, Using split hopkinson pressure bars to perform large strain compression tests on polyurea at low, intermediate and high strain rates, Int. J. Impact Eng. (2008) http://dx.doi.org/10.1016/j.ijimpeng.2008.12.010.

[64] A. Girard, V. Grolleau, D. Mohr, Using miniature cuboidal specimens to determine compression stress–strain curve of sheet metal under static and dynamic loading, Int. J. Solids Struct. 320 (2025) 113527, http://dx.doi.org/10.1016/J.IJSOLSTR.2025.113527.

[65] T. Beerli, C.C. Roth, D. Mohr, Semi-automatic miniature specimen testing method to characterize the plasticity and fracture properties of metals, Acta Mater. 263 (2024) http://dx.doi.org/10.1016/j.actamat.2023.119539.

[66] D. Mohr, G. Gary, B. Lundberg, Evaluation of stress–strain curve estimates in dynamic experiments, Int. J. Impact Eng. 37 (2010) 161–169, http://dx.doi.org/10.1016/j.ijimpeng.2009.09.007.

[67] H. Körber, P. Kuhn, M. Plöckl, F. Otero, P.-W. Gerbaud, R. Rolfes, P.P. Camanho, Experimental characterization and constitutive modeling of the non-linear stress–strain behavior of unidirectional carbon–epoxy under high strain rate loading, Adv. Model. Simul. Eng. Sci. 5 (1) (2018) 1–24, http://dx.doi.org/10.1186/s40323-018-0111-x.